Coupled Generator- and Converter-Modelling for Partly Superconducting Medium-Speed Wind Turbine Generators

Nick Thönelt[1]*, Robin Köster[2], Marc Hiller[1], Yves Burkhardt[2], and Andreas Binder[2]
[1] Institute of Electrical Engineering, Karlsruhe Institute of Technology, Karlsruhe, Germany
[2] Institute for Electrical Energy Conversion, Technical University Darmstadt, Darmstadt, Germany
* nick.thoenelt@kit.edu

Abstract

This work presents a structured modelling and simulation workflow for a medium-speed wind power generator with a superconducting rotor winding and its corresponding power converter. By considering the generator and converter as a coupled drivetrain system, the approach optimizes energy efficiency, material usage, and enables larger wind turbines within existing installation constraints. The effects of the power converter feeding of the normal-conducting stator winding are highly relevant for partly superconducting generators: Even minor additional power dissipation in the cryogenic rotor parts can lead to significant thermal loads for the cryogenic cooling system. This work is part of a current, publicly funded project for the development of a megawatt-scale prototype by 2026. It was found that converter feeding excites additional magnetic field waves in the rotor, causing eddy current losses, which can more than double the losses in the cryogenic rotor, compared to sine current operation. This leads to an impractically large and expensive cooling system, and reduced overall efficiency of the superconducting generator. To examine mitigation measures, finite element calculations with pulsed voltage feeding are carried out, using voltage signals from high-level system simulations.

Keywords – wind generator, synchronous machine, power electronics, IGBT converter, high-temperature superconductor, medium-speed generator

1 Introduction

The increasing demand for renewable energy sources has driven significant advancements in wind power generation technology. In particular, the development of high-power wind turbines necessitates innovative solutions that maximize energy efficiency while minimizing material consumption and operational constraints. One promising approach is the integration of superconducting technology in wind power generators, which enables compact designs and reduces the dependency on rare-earth elements significantly [1]-[2]. This paper introduces a simulation workflow tailored for analysing a superconducting medium-speed wind power generator and its associated power converter. By treating the generator and converter as a unified system, the methodology provides insights into optimizing performance while minimizing resource consumption. Special emphasis is placed on the effects of individual switching actions in the power converter on the distribution of eddy current losses in the generator. A key aspect of this research is the use of finite element analysis (FEA) to develop an accurate generator model and the use of detailed semiconductor-loss models for complete drivetrain efficiency analysis. By establishing a comprehensive simulation environment, this work provides the foundation for a prototype which is currently under construction.

1.1 Finite Element Generator Model

The major novelty of the wind turbine drive train in **Figure 2** consists in a medium-speed, electrically excited synchronous generator with a high-temperature superconducting (HTS) field winding.

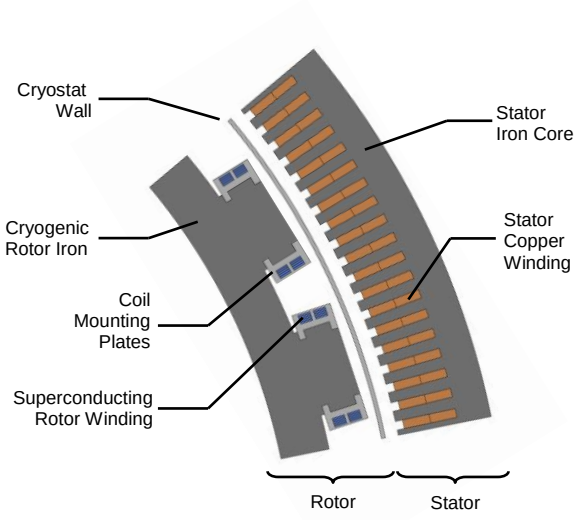

Figure 1 Cross section of a 13 MW, 600 rpm partially superconducting medium-speed generator

The general generator layout, **Figure 1** and **Table 1**, features a cryogenic rotor with cold, massive rotor iron at $T = 30$ K and a single cylindrical cryostat. The superconducting coils are wound around ferromagnetic pole cores. The warm stator features a three-phase, two-layer winding in open stator slots.
In the workflow in **Figure 2**, FEA is used for two modelling steps:

1) Calculation of flux linkage maps of the electrically excited synchronous generator as prerequisite for the drivetrain system simulation: This constitutes a standard problem with typical demands on spatial and time resolution. As a special feature, the high iron saturation

due to the superconducting excitation leads to strongly non-linear flux linkages in the relevant operating range.

2) Calculation of additional eddy current losses in the rotor: This represents a multi-scale problem in terms of I) spatial resolution, i.e. large generator dimensions, **Table 1**, vs. small eddy current regions, and II) time resolution, i.e. long settling times vs. high-frequency eddy current responses due to inverter feeding.

For enabling long simulation times with sufficient time resolution, as required for modelling step 2), 2D FE models with an optimized, structured mesh are used. The transient time stepping simulations in the commercial software *JMAG* 22 are either current-fed with sinusoidal stator currents (step 1) or feature a stator voltage feeding (step 2). The latter is modelled with voltage sources in the circuit that impress the pulsed voltage patterns generated by the drivetrain system simulation, **Figure 2**.

Table 1 Specifications of the medium-speed generator

Outer / air gap diameter $\boldsymbol{d_{so}}$ / $\boldsymbol{d_{\delta}}$	1.8 m / 1.5 m
Pole count $\boldsymbol{2p}$ / stator phase count $\boldsymbol{m_s}$	24 / 3
Active iron length $\boldsymbol{l_{Fe}}$ / pole pitch $\boldsymbol{\tau_p}$	320 mm / 190 mm
Magnetic air gap width $\boldsymbol{\delta_m}$	35 mm
Rated power $\boldsymbol{P_N}$ / speed $\boldsymbol{n_N}$ / stator el. frequency $\boldsymbol{f_{sN}}$	13 MW / 600 rpm / 120 Hz
Rated stator voltage $\boldsymbol{U_{sN}}$ / current $\boldsymbol{I_{sN}}$ / power factor $\boldsymbol{\cos\varphi_{sN}}$	750 V / 10 kA / 1.0
Rated rotor MMF per pole $\boldsymbol{\theta_{f,pol,N}}$	77.4 kA

The HTS field winding is represented by coil regions with homogeneous, impressed current density. No detailed HTS coil model is employed for computational feasibility and since the model uses the A-Formulation [3], where incorporating the power-law characteristic $J(E)$ of current density over electric field strength of the HTS is problematic. Equilibrating the model to steady state conditions in step 2 for the extraction of meaningful additional rotor losses poses a major challenge: The initial turn-on of the rotor excitation leads to a slowly settling eddy current response (>50 el. periods) in the stainless steel cryostat wall (el. conductivity $\kappa = 1.3$ MS/m), the rotor pole cores and the rotor yoke (low temperature steel, $\kappa = 8.3$ MS/m). Moreover, the inherent settling times in stator voltage feeding are elongated for pulsed voltages with rms time harmonics $V_{s,\nu>1}$ of order ν. A two-step procedure is employed:

1) The conductivities κ of all rotor parts are linearly increased on over 30 el. periods.
2) The simulations start with only the stator voltage fundamental $V_{s,\nu=1}$. After 10 el. periods, a smooth transition over 30 el. periods to the pulsed voltage involving all time harmonics is defined. To construct this time series, the voltage signal from the drivetrain system simulation is Fourier transformed and a scaling parameter $\lambda \in [0, 1]$ for harmonics $\lambda \cdot V_{s,\nu>1}$ is introduced.

After this equilibration phase, the time step is reduced to generate the time series for further analyses. The eddy current losses in the cold rotor iron and the cryostat wall are finally determined as time averages over two electrical periods after complete settling to steady state.

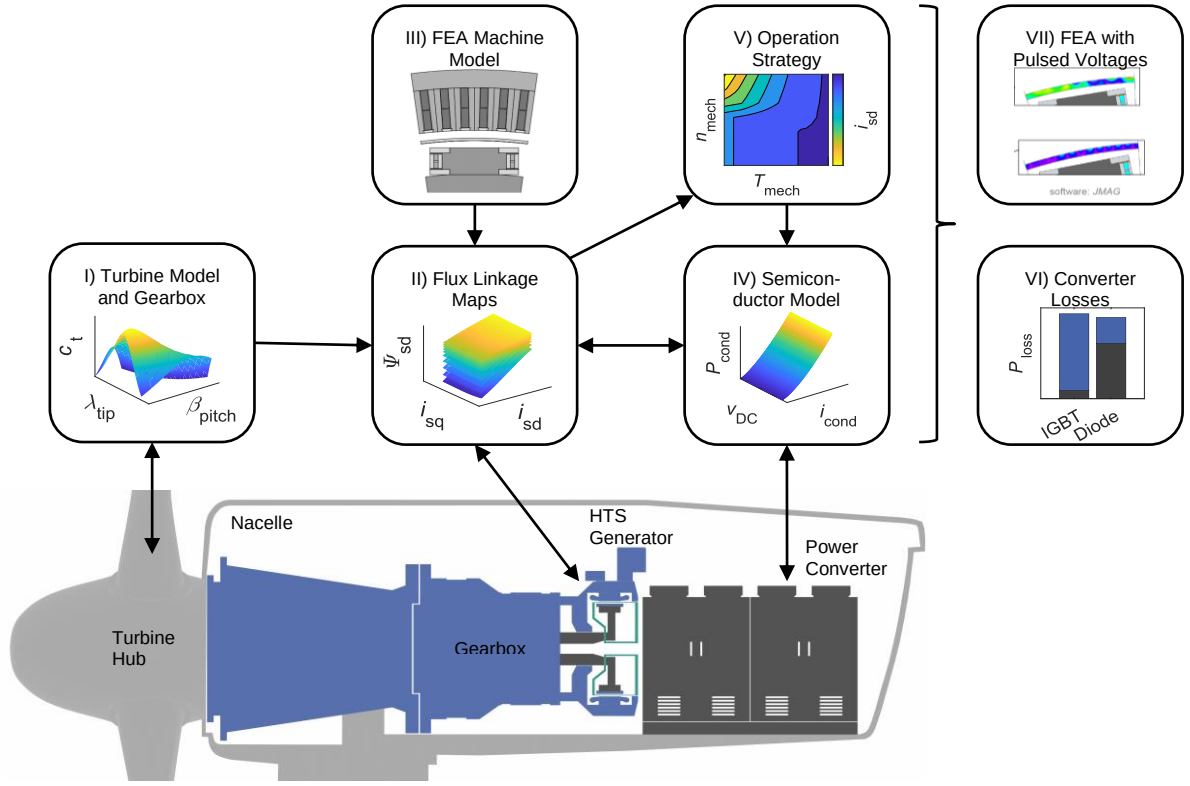

Figure 2 Schematic of modelling and simulation workflow for a wind turbine drivetrain (I) λ_{tip}: tip-speed ratio; β_{pitch}: pitch angle; c_t: torque coefficient; II) Ψ_{sd}: d-axis stator flux linkage; i_{sd}, i_{sq}: d- and q-axis stator current; IV) P_{cond}: conduction losses; i_{cond}: conduction current; v_{DC}: DC link voltage; V) n_{mech}: generator rotational speed; T_{mech}: generator torque, VI) P_{loss}: power loss)

For retrieving the flux linkage maps for a) the stator winding in d- and q-axes $\Psi_{\mathrm{sd}}, \Psi_{\mathrm{sq}}$, and b) the HTS field winding Ψ_{re}, the stator current components i_{sq}, i_{sd}, and the rotor field current i_{Rf} are varied on a regular current grid. Here, a range of $i_{\mathrm{rf}} \in [0, 1.5]$ kA with 11 grid points, $i_{\mathrm{sd}} \in [-15, 0]$ kA with 11 points, and $i_{\mathrm{sq}} \in [-15, 0]$ kA with 11 points is varied. The total number of 1331 calculated operating points ensures well-defined flux mappings for the drivetrain system simulations, as indicated with a visual representation in **Figure 4**. The flux linkages $\Psi_{\mathrm{sd}}, \Psi_{\mathrm{sq}}$ are determined from the time-fundamentals ($k = 1$) of the stator phase flux linkages after steady-state operation is established.

1.2 Power Converter Model

The power losses in a state-of-the-art three-phase, two-level voltage source converter using IGBTs are analysed by evaluating both conduction and switching losses in the semiconductor devices. The analysis is based on phase current waveforms from a coupled drivetrain model described in Section 2.2 and key system parameters, including the number of parallel devices, the DC-link voltage, and operating temperature of the semiconductors from a thermal network. The energy loss characteristics of the transistor T and diode D are obtained from experimentally validated loss models from the semiconductor manufacturer [4], which describe the dependency of switching and conduction losses on the current, voltage, and junction temperature ϑ of a device. Switching and recovery losses are determined by detecting zero-crossing points in the transistor and diode current waveform and by integrating the turn-on and turn-off energy dissipation per switching event. The total switching losses of the transistor can be expressed as:

$$P_{\mathrm{sw,\,T}} = \frac{1}{T_{\mathrm{el}}} \sum_{k=1}^{N_{\mathrm{sw}}} \Big(E_{\mathrm{on},k}\big(i_{\mathrm{T}}(t), \vartheta_{\mathrm{T}}(t)\big) + E_{\mathrm{off},k}\big(i_{\mathrm{T}}(t), \vartheta_{\mathrm{T}}(t)\big) \Big) \tag{1}$$

where $E_{\mathrm{on},\,k}$ and $E_{\mathrm{off},\,k}$ denote the turn-on and turn-off energy losses at the k-th switching event, N_{sw} is the total number of switching events within the electrical period T_{el}. A similar formulation is applied to the diode recovery losses $P_{\mathrm{rec,\,D}}$, considering the recovery energy $E_{\mathrm{rec},\,k}$. Conduction losses are calculated by integrating the instantaneous power dissipation over the conduction period, yielding

$$P_{\mathrm{cond,T}} = \frac{1}{T_{\mathrm{el}}} \int_0^{T_{\mathrm{el}}} v_{\mathrm{T}}\big(i_{\mathrm{T}}(t), \vartheta_{\mathrm{T}}(t)\big) \cdot i_{\mathrm{T}}(t)\,\mathrm{d}t \tag{2}$$

for the transistor, where v_{T} is the conduction voltage drop as a function of the current i_{T} and the junction temperature ϑ_{T}. The same approach is applied to the diode conduction losses $P_{\mathrm{cond,\,D}}$, considering the corresponding conduction voltage characteristic. The total converter losses are obtained by scaling the per-device losses according to the number of parallel devices and phases in the system. Identical electrical and thermal characteristics are assumed for all parallel semiconductor devices.

Results for two different operation strategies of the generator as well as modulation schemes of the power converter are presented in Section 3.1, illustrating the contributions of transistor losses $P_{\mathrm{cond,\,T}}$ and $P_{\mathrm{sw,\,T,}}$ as well as diode losses $P_{\mathrm{cond,\,D}}$ and $P_{\mathrm{rec,\,D}}$. This analysis provides valuable insights into the dominant loss mechanisms, supporting the optimization of power semiconductor design for the application in medium-speed wind turbines and thermal management strategies in high-power converter applications.

1.3 Turbine Characteristic

Furthermore, this work incorporates a turbine model adapted from the International Energy Agency (IEA) *Wind 15-Megawatt Offshore Reference Wind Turbine* [5], ensuring that investigated drivetrain operating points align with real-world operating conditions occurring in offshore turbines for steady state, as illustrated in **Figure 3**.

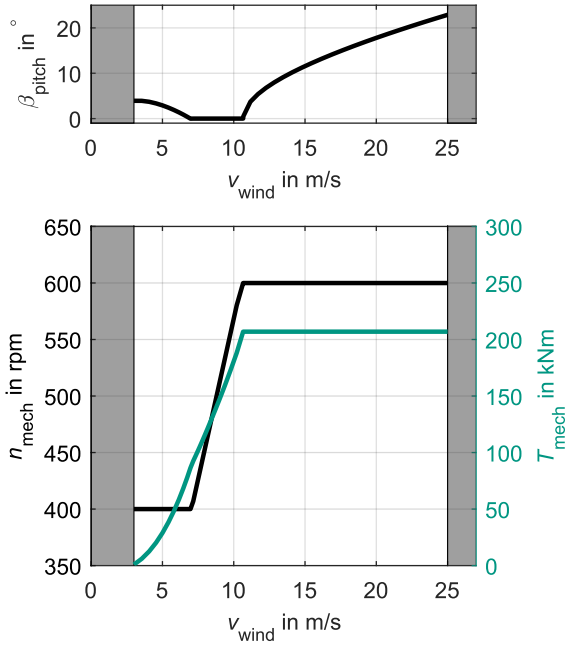

Figure 3 Turbine pitch angle β_{pitch} (top) [5], rotational speed n_{mech} and mechanical torque T_{mech} of the generator (bottom) over the wind speed v_{wind} between cut-in and cut-out wind speed (white background)

2 Integrated Drivetrain System Simulation Environment

2.1 Operation Strategy

In order to investigate the influence of the operation strategy of the generator on the combined drivetrain, two main strategies are calculated offline from the flux linkage maps of the FEA model: a) maximum torque per ampere (MTPA) and b) unity power factor ($\cos\varphi = 1$). Particularly for partially superconducting generators, the ohmic rotor resistance R_{r} is multiple orders of magnitude smaller than the time-fundamental stator resistance R_{s}. A ratio of $\frac{R_{\mathrm{r}}}{R_{\mathrm{s}}} = 0.012$ is assumed for the investigated generator and will be measured in future work on the full-scale prototype.

a) MTPA strategy minimizing loss function F:

$$\min F(i)_{i\in R^3} = \frac{3}{2}\cdot R_\mathrm{s}\cdot\left(i_\mathrm{sd}^2 + i_{sq}^2\right) + R_\mathrm{r}\cdot i_\mathrm{rf}^2 \qquad (3)$$

s.t.

$$v_\mathrm{sd} = R_\mathrm{s}\cdot i_\mathrm{sd} - p\cdot\omega_\mathrm{mech}\cdot\Psi_\mathrm{sq}\left(i_\mathrm{sq}, i_\mathrm{sd}, i_\mathrm{rf}\right)$$
$$v_\mathrm{Sq} = R_\mathrm{s}\cdot i_\mathrm{sq} + p\cdot\omega_\mathrm{mech}\cdot\Psi_\mathrm{sd}\left(i_\mathrm{sq}, i_\mathrm{sd}, i_\mathrm{rf}\right)$$
$$v_\mathrm{rf} = R_\mathrm{rf}\cdot i_\mathrm{rf}$$

linear inequality constraints:

$$0 > |v_\mathrm{rf}| - v_\mathrm{rf,max}$$
$$0 > |i_\mathrm{rf}| - i_\mathrm{rf,max}$$

nonlinear inequality constraints:

$$0 > \sqrt{i_\mathrm{sd}^2 + i_\mathrm{sq}^2} - i_\mathrm{max}$$
$$0 > \sqrt{v_\mathrm{sd}^2 + v_\mathrm{sq}^2} - v_\mathrm{max}$$

nonlinear equality constraints:

$$0 = \frac{3}{2}\cdot p\cdot\left(\Psi_\mathrm{sd}\cdot i_\mathrm{sq} - \Psi_\mathrm{sq}\cdot i_\mathrm{sd}\right) - T_\mathrm{mech}$$

b) Unity power factor strategy as a) with additional nonlinear equality constraint:

$$\gamma = \pi + \arctan\left(\frac{i_\mathrm{sd}}{i_\mathrm{sq}}\right)$$
$$\vartheta = \arctan\left(\frac{v_\mathrm{sd}}{v_\mathrm{sq}}\right)$$
$$0 = (\gamma - \vartheta) - \pi$$

The underlying interpolated flux linkage maps are visualized on the d- and q-axis stator current-plane for 11 discrete current values of the electrically excited rotor for $i_\mathrm{rf} \in [0, 1.5]$ kA as presented in **Figure 4**. Furthermore, results of the MTPA offline optimization for a regular mesh in the T_mech-n_mech-plane consisting of 400 points are presented in **Figure 5** including the trajectory according to the turbine characteristic presented in Section 1.3.

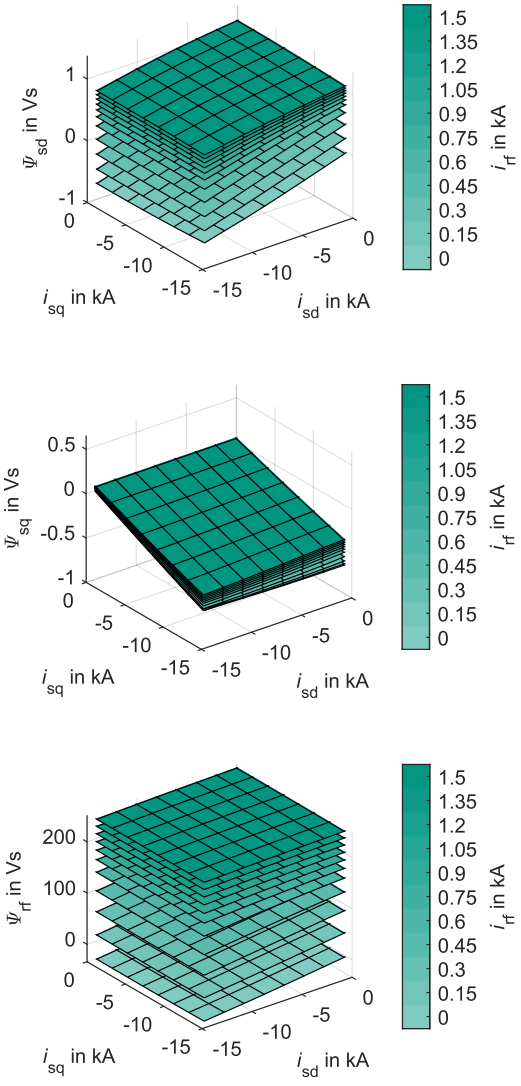

Figure 4 Simulated flux linkage maps of the stator d- and q-axes Ψ_sd, Ψ_sq, and rotor flux linkage Ψ_rf, resulting from FEA model for discrete excitation current values i_rf

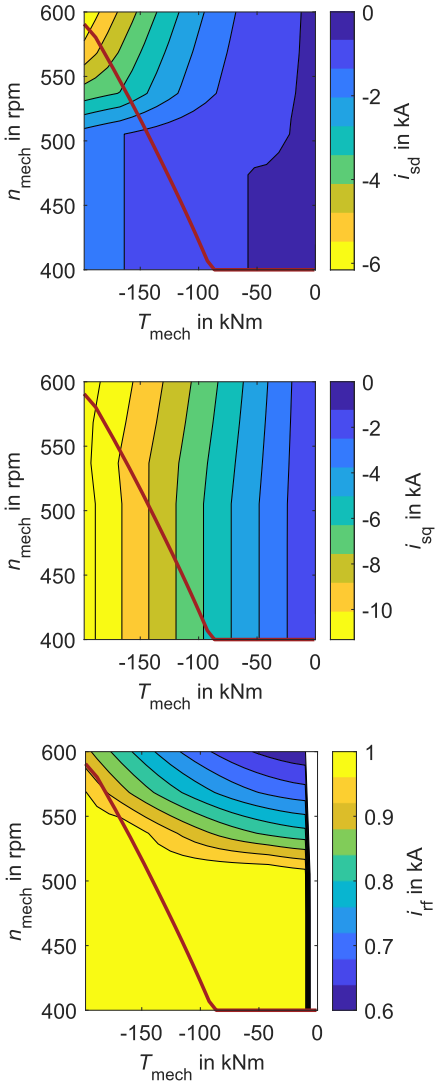

Figure 5 MTPA optimal operating points for the stator current components i_sd, i_sq, and the rotor excitation current i_rf along the trajectory of the according turbine model (red)

2.2 Drivetrain Model

The power converter model described in Section 1.2 is solved numerically and coupled with the machine model based on flux linkage maps from FEA represented in voltage equations (4)-(6) for the stator d- and q-axis as well as the field winding at each timestep. Adopted from [6], R_s and R_r represent the ohmic resistances of the stator and rotor, p the number of pole pairs and ω_mech the mechanical angular speed of the generator.

$$v_\mathrm{sd} = R_\mathrm{s} \cdot i_\mathrm{sd} + \frac{\mathrm{d}\Psi_\mathrm{sd}}{\mathrm{d}t} - p \cdot \omega_\mathrm{mech} \cdot \Psi_\mathrm{sq} \tag{4}$$

$$v_\mathrm{sq} = R_\mathrm{s} \cdot i_\mathrm{sq} + \frac{\mathrm{d}\Psi_\mathrm{sq}}{\mathrm{d}t} + p \cdot \omega_\mathrm{mech} \cdot \Psi_\mathrm{sd} \tag{5}$$

$$v_\mathrm{rf} = R_\mathrm{r} \cdot i_\mathrm{rf} + \frac{\mathrm{d}\Psi_\mathrm{rf}}{\mathrm{d}t} \tag{6}$$

One major benefit of the presented workflow is detailed analysis at small timescales using FEA and the possibility to evaluate effects on annual energy production with limited computational effort for given wind speed datasets.

3 Coupled Drivetrain Effects

The modulation scheme of the power converter plays a critical role in determining both the semiconductor switching behaviour and the distribution of magnetic field waves within the generator. In the presented partly superconducting generator topology the applied scheme of modulation directly influences the distribution and spectral content of the stator current waveforms. This, in turn, affects both the power dissipation in the semiconductor devices and the eddy current losses in the cryostat wall as well as in cryogenic parts of the rotor structure. System-level electromagnetic transient simulations were performed to generate true-to-application voltage and current waveforms for different modulation schemes, including:

a. super-sine with converter zero-to-neutral voltage v_N0:

$$\vec{v} = (v_{phase\,1}, v_{phase\,2}, v_{phase\,3}) \tag{7}$$

$$v_{N0,\mathrm{super}} = -\frac{\max(\vec{v}) + \min(\vec{v})}{2} \tag{8}$$

b. flat-top with converter zero-to-neutral voltage:

$$v_{N0,\mathrm{flat}} = \begin{cases} \frac{v_\mathrm{DC}}{2} - \max(\vec{v}), \forall |\max(\vec{v})| > |\min(\vec{v})| \\ -\frac{v_\mathrm{DC}}{2} - \min(\vec{v}) \quad \text{, otherwise} \end{cases} \tag{9}$$

The pulsed voltage waveforms were subsequently used as feeding sources in time-domain finite element models of the generator, enabling detailed evaluation of the resulting eddy current loss distributions.

Although not considered in this work, the impact of the modulation scheme and the resulting torque ripple on mechanical components of the drivetrain is particularly interesting for partly superconducting generators. A key component for mechanical power transfer in such machines is the torque-transmission-element (TTE) connecting the cryogenic rotor to the warm mechanical shaft. The impact of high frequency oscillatory torque components on the TTE can also be investigated with the proposed coupled drivetrain approach in future work. In Subsection 3.1, initial results for two exemplary cases are presented.

3.1 Influence of the Modulation Scheme on the Semiconductor Power Losses and Eddy Current Losses

Due to the sensitivity of cooling power to additional thermal loads at low temperatures, even relatively small increases in rotor power losses can result in disproportionately high demands of cryogenic system power. Eddy-current losses at cryogenic temperature take a coefficient of performance (COP) of 1.3% for a state-of-the-art Gifford-McMahon cryocooler into account [7], while eddy-current losses in the cryostat wall are removed by the air flow in the air gap. Simulation results based on the described modelling approach reveal how conventional pulse-width modulation schemes introduce high-frequency harmonics with different spectral content into the airgap magnetic flux density, which penetrate the cryostat wall and induce significant eddy currents in the non-superconducting metallic structures inside the cryostat, such as coil mounting plates, yoke and pole core. These losses are particularly problematic due to their location within the cryogenic environment, where cooling power is both limited and costly. The simulation results show that under different modulation schemes and operating strategies, eddy current losses in the rotor result in a. 12.3 kW or b. 15.7 kW of electrical compressor power of the cryogenic system compared to 0.9 kW in case of ideal sinusoidal feeding due to the effect of spatial harmonic field waves resulting from the switching transitions of the power converter, as shown in **Figure 6**.

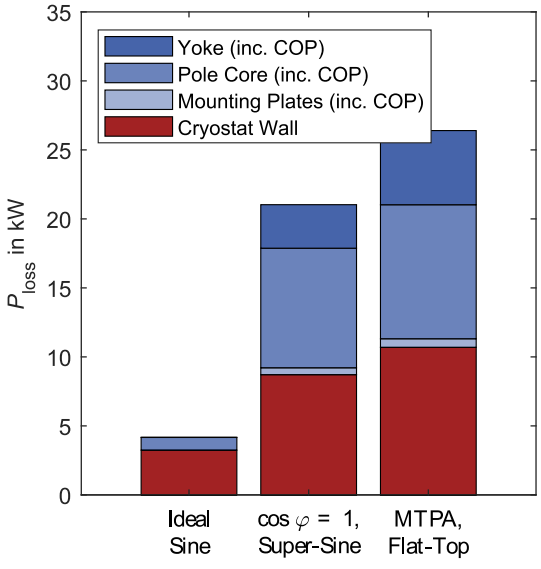

Figure 6 Eddy-current losses at rated 13 MW, 600 rpm of the generator rotor at unity power factor with super-sine modulation (b), a.) or at MTPA with flat-top modulation (a), b.) considering the cryocooler COP

Simultaneously, the semiconductor conduction and switching losses were evaluated for each modulation method. While advanced schemes such as flat-top modulation can reduce switching losses in the converter by 18.4 kW, as shown in **Figure 7**, they induce increased rotor eddy current losses resulting in 3.4 kW additional compressor power for the cryogenic system. This trade-off necessitates a co-optimization approach in which the modulation strategy is chosen not only to minimize converter losses but also to limit thermal loads of the cryogenic system.

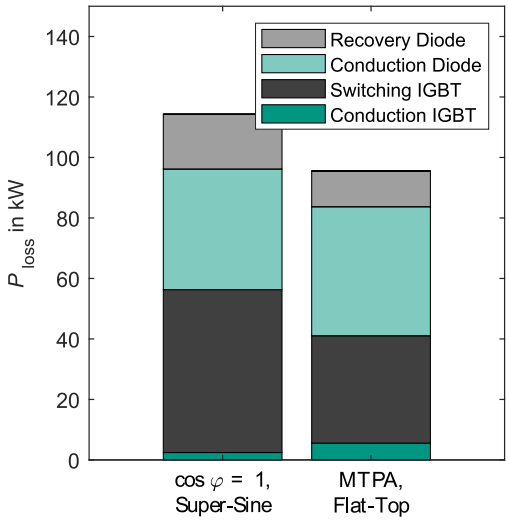

Figure 7 Results of drivetrain loss analysis at rated 13 MW, 600 rpm of the power converter rotor at unity power factor with super-sine modulation (b), a.) or at MTPA with flat-top modulation (a), b.)

The results emphasise the importance of harmonizing electrical feeding strategies with the thermal and electromagnetic constraints of superconducting generator technology. It was observed that a significant portion of the eddy current losses induced by converter harmonics occurs not only in the cryogenic rotor components but also in the warm cryostat wall as presented in **Figure 6**. These losses could potentially lead to localized overheating in the warm section of the air gap, which can elevate the temperature of the normal-conducting stator winding, further influencing efficiency. With respect to overall drivetrain efficiency, initial results indicate that the combination of the MTPA operation strategy and flat-top modulation is preferred for the presented generator and converter design. However, this results in comparatively high cryocooler investment costs. A reallocation of these cryogenic system costs could enable enhanced power converter efficiency or implementation of advanced converter topologies. Furthermore, the integration of a dedicated copper damper screen [8] can be applied in order to reduce losses at cryogenic temperature.

4 Conclusion

This work presents a comprehensive modelling and simulation workflow for the coupled analysis of a partly superconducting medium-speed wind turbine generator and its according power converter. By considering detailed semiconductor loss models with electromagnetic finite element simulations of a partly superconducting generator, the presented approach enables evaluation of drivetrain losses. First results show that while advanced modulation schemes, such as flat-top modulation, can significantly reduce switching losses in the converter, they introduce additional high-frequency harmonics current into the machine. These harmonics lead to a substantial increase in eddy current losses within both the cryogenic rotor components and the warm cryostat wall. The resulting thermal load, particularly in the cryogenic rotor can outweigh the benefits of reduced semiconductor losses depending on thermal constraints of the superconducting rotor system. These findings emphasize the necessity for a co-optimization of converter modulation schemes and generator operation strategies, taking into consideration efficiency and the thermal constraints inherent to superconducting technology. Future work will investigate optimized pulse patterns, with the aim of reducing losses in rotor parts at cryogenic temperatures without compromising converter efficiency and while mitigating overheating of the cryostat wall. Furthermore, the use of advanced converter topologies, such as three-level active neutral point clamped (ANPC) converters and their modulation schemes, will be investigated.

The authors acknowledge the financial support of this work by the German Federal Ministry for Economic Affairs and Climate. (03EE3094C)

5 References

[1] M. Tinkham, Introduction to Superconductivity, 2nd ed. New York, NY, USA: Dover Publications, 2004, p. 316.

[2] R. H. Petrucci, F. G. Herring, J. D. Madura, and C. Bissonnette, General Chemistry: Principles and Modern Applications, 11th ed. Boston, MA, USA: Pearson, 2016, pp. A30-A33.

[3] R. Köster, “Direct Drive Wind Generators with Superconducting Excitation in the Multi-MW Class”, Dissertation, Technical University Darmstadt. 2023.

[4] Dataset “FF1700XTR17IE5D - PLECS”, Munich, Germany, Infineon Technologies AG, 2023.

[5] E. Gaertner et al., “Definition of the IEA 15-Megawatt Offshore Reference Wind”, Golden, CO, National Renewable Energy Laboratory, 2020.

[6] P. Winzer, J. Richter and M. Doppelbauer, "Dynamic control of generalized electrically excited synchronous machines using predictive flux control", Florence, Italy, 2016, pp. 2772-2777

[7] Technical Specification “AL325 Gifford-McMahon Cryocooler”, Bluefors Cryocooler Technologies Inc., 2024.

[8] R. Köster and A. Binder, “Damper Screen Design in HTS Medium Speed Wind Generators Considering Stator Current Harmonics,” 2024 International Symposium on Power Electronics, Electrical Drives, Automation and Motion (SPEEDAM), Napoli, Italy, 2024, pp. 593-599